Neutral Drift and Transport in Ion and Hall Thruster Test Facilities

IEPC-2025-606

Presented at the 39th International Electric Propulsion Conference, Imperial College London, London,
United Kingdom
14-19 September 2025

Richard A. Obenchain* and Richard E. Wirz[†]
Oregon State University, Corvallis, Oregon, 97331, USA

Ion and Hall thruster vacuum facility tests exhibit complex transport of neutral species through the facility that lead to important facility effects. This transport can be thought of as a "neutral drift" ("dynamic pressure") superimposed on the facility "background flux" ("static pressure"). These neutral fluxes can be used to accurately assess flux to the thruster face and thus neutral ingestion as well as the neutral density in the thruster plume. Comparisons of simulations to facility data show that the neutral ingestion to the thruster face can vary considerably between facilities and is affected by facility geometry, beam target design, pumping configurations, and facility pumping performance (e.g., sticking coefficients). For example, comparison of two world-class pumping facilities shows variations of over 30% for conditions at which conventional vacuum gauge measurements show precise agreement. These findings support recommendations to facility operators and designers are to properly place and interpret neutral flux gauges (i.e., vacuum "pressure" gauges) to measure the facility neutral drift and the neutral flux most relevant to neutral ingestion and near-thruster facility-borne neutral density

I. Introduction

Orates and pressure, metrics that are valuable in low-vacuum conditions and have been translated to standards for high vacuum testing.^{1,2} Such metrics are useful within the collisional or fluid regimes of low-vacuum conditions but are less representative as the environment transitions from collisional to collisionless regimes, at which point mass and energy fluxes dominate.³ Angular coefficient methods (ACMs) have long been used to model collisionless flow.⁴⁻⁹ Not only are such methods computationally efficient, the underlying principle of exchanging particles between surfaces best represents the physics inherent to collisionless flow, in which particle behavior is considered to be determined solely by interactions with surfaces and can be considered an exchange of fluxes.¹⁰ Within the field of electric propulsion, ACMs have been applied in 1-D, 2-D, and 3-D forms for electric propulsion simulations, primarily to describe background neutral particle transport through vacuum facilities or discharge chambers;^{6,11-13} such models have been shown to be as accurate as more computationally intensive DSMC models.¹⁴

In 2020, Frieman, Liu, and Walker published a model, based on prior work by Cai, Boyd and Sun, predicting a bulk "background flow" within a test facility during thruster operation. ^{11,12} This model was fundamentally a one-dimensional flux model using simplified ACM. While comparatively easy to implement, the one-dimensional nature of the model prevented in-depth analysis of larger flow characteristics, especially in facilities with complex geometry. Further, the model focused primarily on pump placement relative to the thruster and not the impact of facility geometry or other characteristics.

The objective of this paper is to characterize the neutral flux behavior within EP facilities using 3D simulations to accurately characterize detailed facility effects. To achieve this objective, we have developed

[†]Exec. Dir. for Aerospace Research Programs, College of Engineering, richard.wirz@oregonstate.edu



^{*}PhD. Student, Mechanical, Industrial, and Manufacturing Engineering, obenchar@oregonstate.edu

3-D ACM simulations of two high power electric propulsion test facilities operating under several pump configurations to study neutral transport within the facility. We begin to develop analytical characterization of facilities based on experimental conditions and apply those characterizations to gain understanding of flux patterns within the simulated facilities. We attempt to match thruster environment conditions between two facilities with different geometries as a test case; we also recommend two additional quantities of merit to be presented along with experimental measurements in order to increase reproducibility.

II. Theory

Steady state conditions for vacuum facilities can be found through conservation of mass and energy. In this effort, we focus primarily on mass conservation at steady state, assuming all mass entering the facility (through the thruster, cathode, neutralizer, bleed flows, or other sources) is extracted or captured by pumps. Additionally, particle motion within a collisionless regime is dictated by flux exchange between the interior surfaces of the facility, including the thruster, pumps, target, and all structural surfaces of the facility. For a cyropump operating in high vacuum, the effective extraction area of the pump is defined as A_{ex} , $n = A_n \alpha_{sc}$. The total effective extraction area for the facility is then the sum of all pump extraction areas:

$$A_{ex} = \sum A_{ex,n} = \sum A_n \alpha_{sc} \tag{1}$$

Combining the two prior observations with the flux-based extraction area facility, we can define a background flux λ_{bk} for the experimental condition:

$$\dot{m}_{in} = \lambda_{bk} A_{ex} \tag{2}$$

where \dot{m}_{in} is the mass flow into the facility, A_{ex} is the total effective extraction pump area. The background flux λ_{bk} is then the average flux to pump surfaces needed to maintain the steady state condition under the given mass flow and pump configuration. For an ideal facility with uniform distribution of mass inflow and extraction, all open (non-shadowed) surfaces within the facility would experience the background flux.

Facilities cannot generally reproduce the ideal condition and thus exhibit nonuniform mass flow behavior. Extending the prior observation, all mass entering a facility at a given location must traverse the chamber to reach pumps and be extracted; for sticking coefficients lower than 50%, most particles will need to intersect pump surfaces multiple times before being captured. Thus, pump placement within the facility relative to the mass inflow location(s) will drive a bulk particle drift within the facility as mass migrates from its point of entry to its point of extraction. This drift may be observed as an increase in flux to surfaces along the drift path. In simplified terms and assuming one-dimensional motion, the magnitude of the drift flux at any location z along the drift path from one source to pump n may be approximated as:

$$\lambda_{dr,src:n}(z) = \frac{A_{ex,n}}{A_{ex}} \frac{\dot{m}_{in,src}}{A_{cs}(z)}$$
(3)

where $A_{cs}(z)$ is the cross-sectional area of the facility at z and $\dot{m}_{in,src}$ is the total mass flow from that source. The total drift past any location z is then the net sum of the drift fluxes accounting for directionality of the flux:

$$\lambda_{dr}(z) = \sum_{source\ pump} \lambda_{dr,src:n}(z) \tag{4}$$

Figure 1 depicts a simplified flow environment. The overall facility (center) exhibits both the general background flux λ_{bk} against all surfaces and an additional drift flux λ_{dr} representing the bulk motion of mass from the source on the right to the sink on the left as shown in Figure 1. The difference in flux between the source (right) and sink (right) is the drift flux, with the average flux within the chamber being the background flux. The flux to the wall at the source is the background flux minus one half the drift flux, as the drift flux is moving away from the wall and thus reducing it. The flux to the wall at the sink is the sum of the background flux and one-half the drift flux, as the drift is moving towards it. Walls on the top and bottom of the facility will generally experience a flux equal to the background flux. Similarly, Figure 2 depicts the flux impacts on the thruster itself. The thruster face experiences an increase in flux due to drift moving towards it, while the thruster rear experiences a decrease in flux as drift moves away from it. The thruster sides are perpendicular to the direction of the drift flux and experience only the characteristic flux.



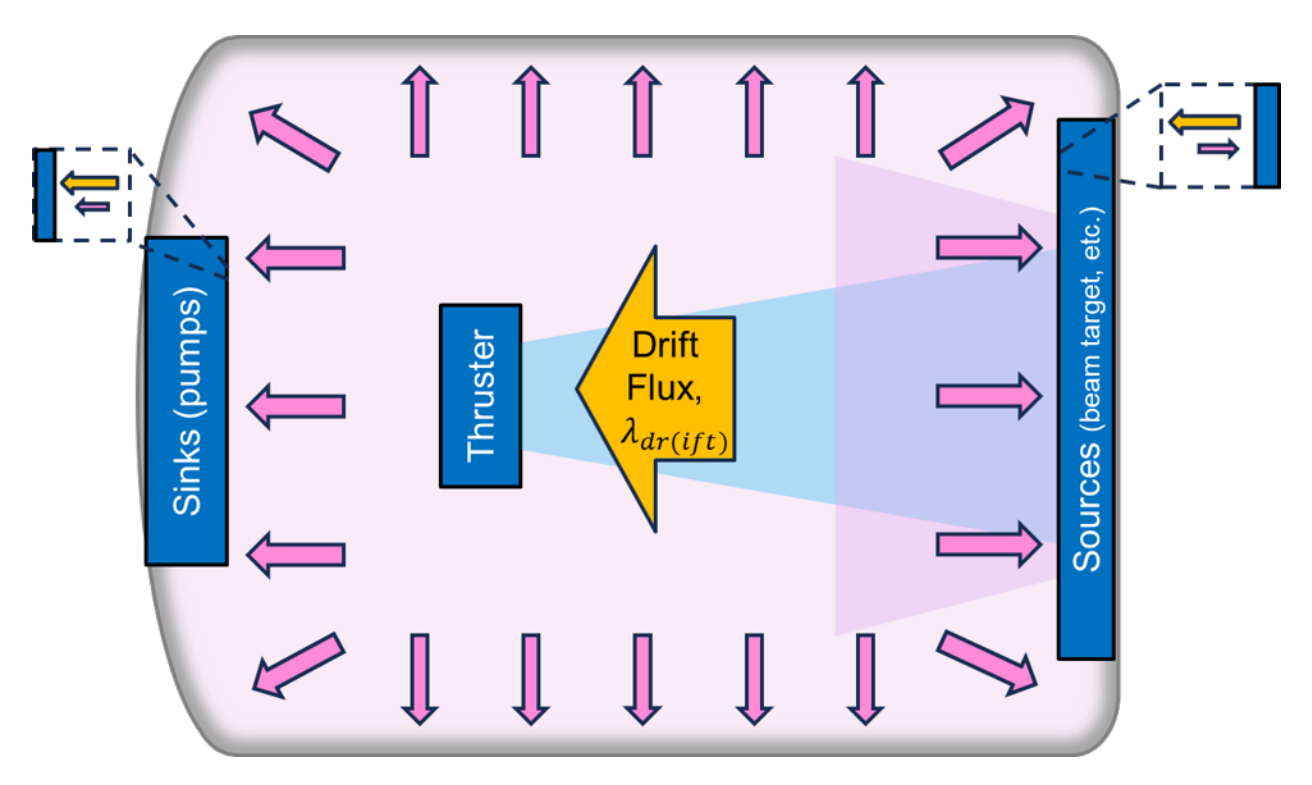


Figure 1: Depictions of background and drift fluxes in the facility. For thruster surfaces, the flux to the thruster face is the background flux plus a geometrically determined portion of the drift flux, as the drift is in the direction of the face; at the rear, the drift is moving away from the surface, so the flux to the rear is the background flux minus a portion of the drift flux.

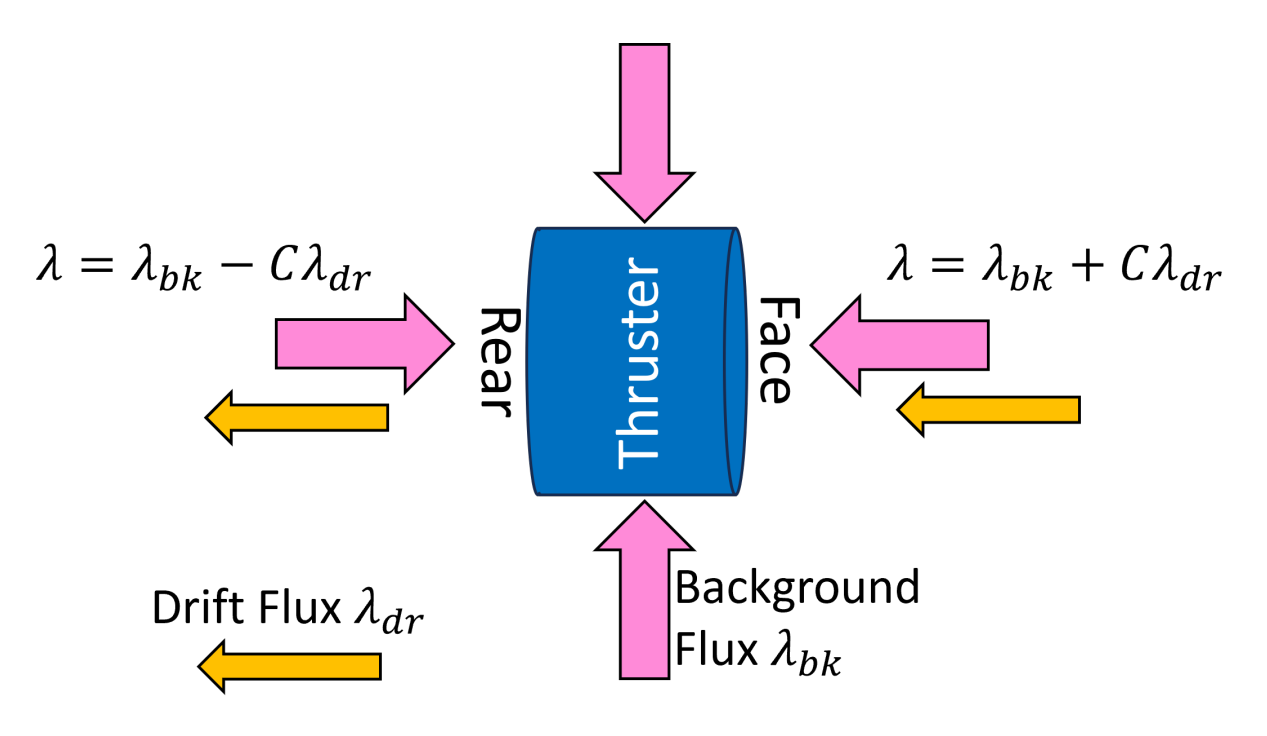


Figure 2: Depictions of background and drift fluxes in the thruster's local environment. Neutrals entering the facility will generate both the background flux λ_{bk} against all surfaces and the drift flux λ_{dr} directionally from the source(s) to the sink(s).



Two facilities configured to identical mass flow and pump configurations relative to the thruster location should therefore produce similar flux to the thruster face and particle densities near the thruster. Note that all three conditions must be satisfied: while scaling mass flow and extraction may reproduce the same background flux, the drift between inflow and extraction will be higher under higher mass flow conditions and lead to changes in flux to surfaces along the drift path; further, the positions of pumps relative to the thruster must be approximately the same to ensure similar drift paths. Therefore, inflow and extraction configurations must be maintained to reproduce the same near-thruster environment.

III. Methods

A. Facilities

As part of the JANUS Facility Interpolation Tests (designated FIT1 and FIT2), computational simulations of two test facilities were created incorporating ACM-based free molecular flow for neutral transport and thermal exchange between surfaces. For FIT1, tests were performed in Vacuum Test Facility 2 (VTF-2) at the Georgia Institute of Technology's High Power Electric Propulsion Laboratory; FIT2 was conducted in the Large Vacuum Test Facility (LVTF) at the University of Michigan's Plasmadynamics and Electric Propulsion Laboratory. While both facilities are intended and used for high power electric propulsion testing, VTF-2 and LVTF have very different facility geometries. Additionally, both facilities utilize TM1200i cryopumps: VTF-2 solely relies on 10 TM1200i cryopumps, while LVTF uses up to 13 TM1200i cryopumps and 5 custom cryopanels. This similarity presents the opportunity for isolation of mass extraction capability from facility geometry.

Additional details are relevant for VTF-2. Figure 3 shows the numbering of the 10 TM1200i pumps as used in this study and the designations for referencing thruster surfaces. In the VTF-2 simulations, beam ions are released as thermalized neutrals from the conical beam target, rear facility wall, and the conical fustrum colloquially referred to as the converger.

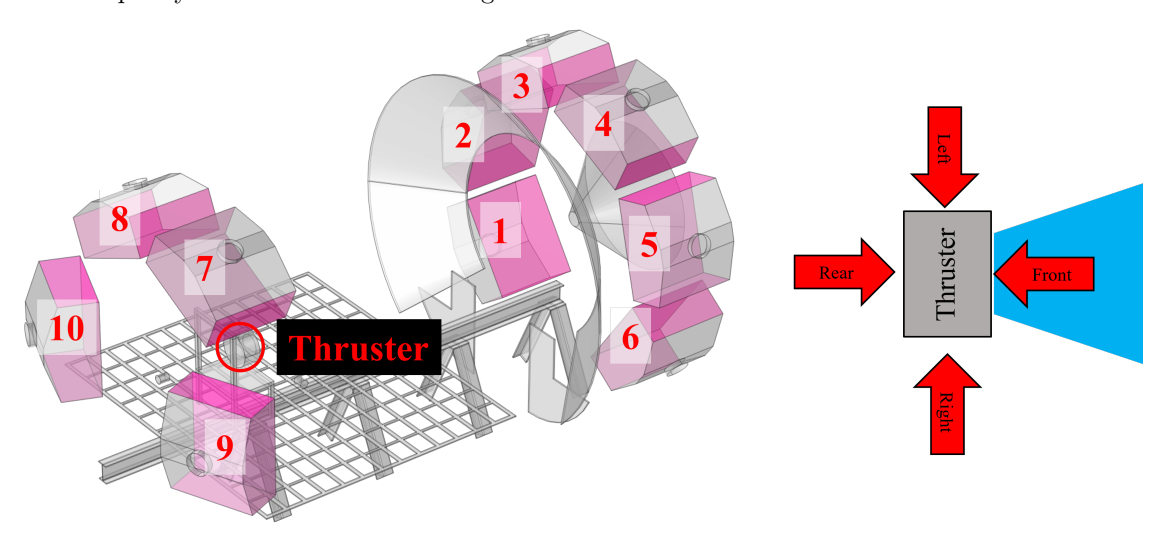


Figure 3: Left, pump positioning and numbering for the VTF-2 facility. The thruster position is circled in red. Right, a top-down reference for the thruster showing the designations for front, left, rear, and right sides.

For each chamber, 3 separate pump configurations consisting of 4 total TM1200i pumps were identified: one with all four pumps downstream of the thruster (4 Down), one with all four pumps upstream of the thruster (4 Up), and one with 2 pumps downstream and 2 pumps upstream (2 Up 2 Down); see Figure 4. The TM1200i has an effective pumping surface of $2.7m^2$ and an approximate sticking coefficient of 0.26; the sticking coefficient is assumed to be a characteristic of the pump itself as long as the cryo surfaces are not thermally saturated. The TM1200i has an external LN2-cooled "shroud" maintained at an operating temperature of approximately 160K; during simulations, the shroud temperatures are maintained even when the pump itself is considered as inoperative to reflect actual experimental conditions and maintain the thermal



characteristics of the facility. For LVTF, disabling the 5 cryopanels includes disabling cooling on the panels, resulting in the panels reaching the average chamber temperature. Each configuration was simulated using the same thruster operational characteristics; resulting fluxes and densities at several key locations within the facility were then reported by the simulation.

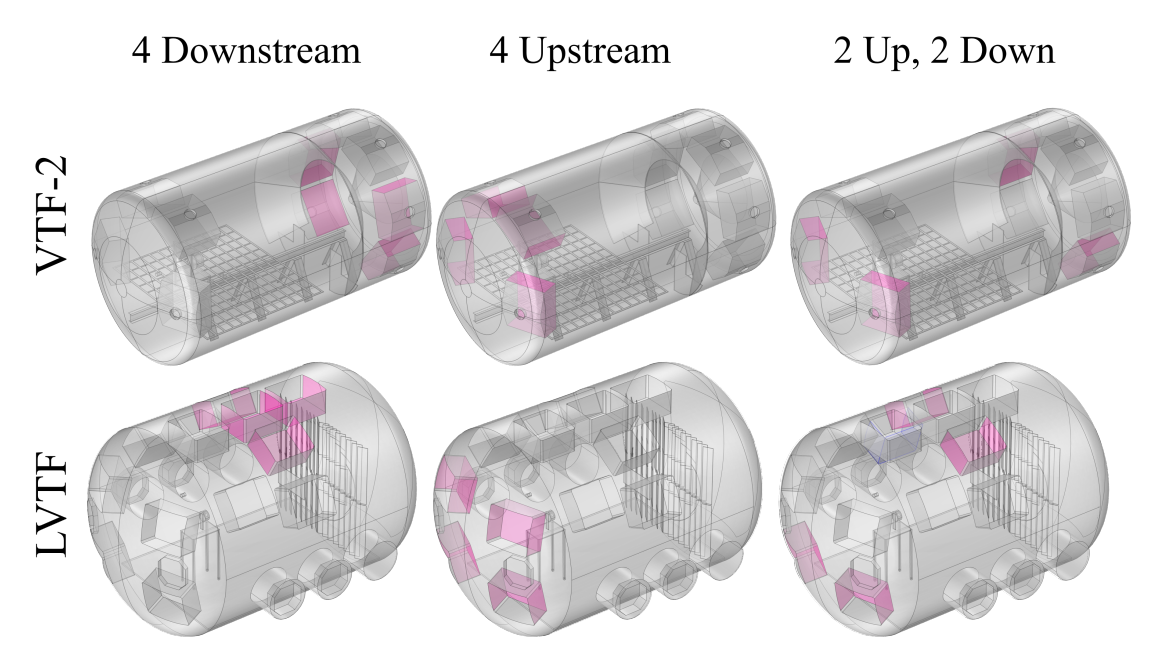


Figure 4: The 6 pump configurations used in the simulations. Each configuration has four active TM1200i cryopumps, ensuring that the total pumping capacity of the simulation remains constant.

B. Thruster

The simulated thruster was the H9 Hall Effect Thruster used during the FIT experiments. The primary thruster characteristics incorporated into the simulation were the thruster physical geometry, beam profile, mass flow, propellant efficiency, and thruster body temperature. For the purposes of this study, thruster characteristics were not critical; the only requirement was that characteristics remained consistent across all simulation conditions. Use of the H9 was for ease of implementation as well as potential comparisons to future experiments that may be performed to corroborate the findings.

The thruster beam was simulated using a two-source approximation described previously;¹³ Figure 5 depicts the two-source approximation for VTF-2. Beam ions are not directly simulated but are instead considered released as accommodated neutrals from the target surfaces based on the beam profile distribution. Neutrals lost from the thruster or passing through the cathode are emitted diffusely from the thruster surface. Thermal loading of thruster and target surfaces is simulated by setting these surfaces to temperatures gathered through the FIT experiments.

For all simulations, mass flow through the thruster was set to 13.6mg/s xenon, with 10% exiting the thruster as leakage or through the cathode. Temperatures within the facilities were defined using prior experimental results for the H9 operating under 300V and 15A.

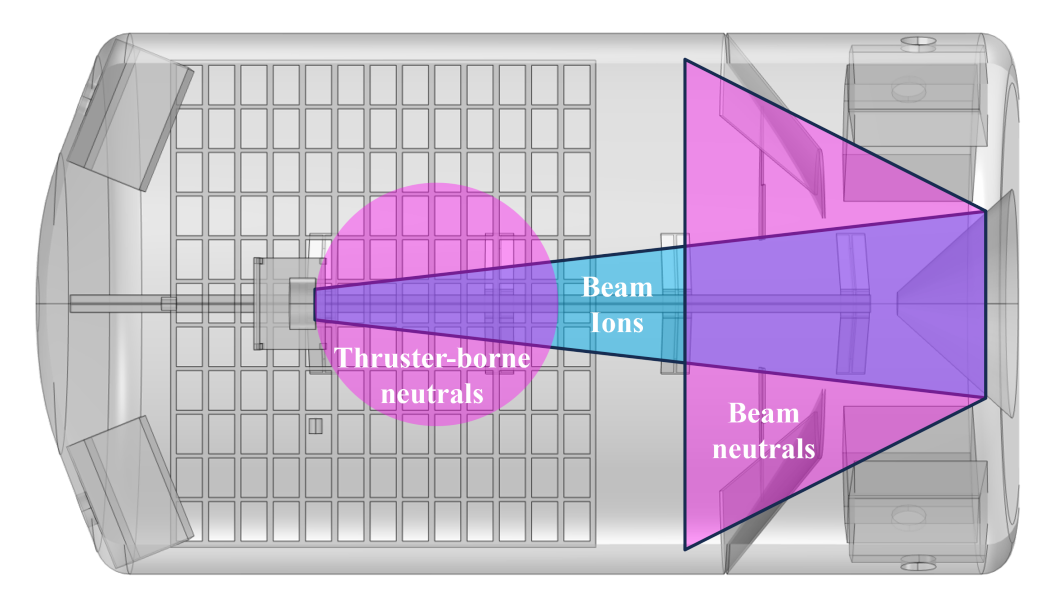


Figure 5: The two source approximation for VTF-2. Neutrals are considered as entering the facility from two locations: neutrals lost from the thruster or passing through a cathode or neutralizer (thruster-borne neutrals) are considered as emitted from the thruster face; beam ions are not directly simulated but assumed to impact the target and nearby surfaces and are considered to enter the facility as neutrals emitted from the target surfaces (beam neutrals).

IV. Results

Two separate analyses were performed: one study of flow behavior within VTF-2 for the three 4-pump configurations, and one comparing results between VTF-2 and LVTF.

A. VTF-2 Flux

All three pump configurations were simulated. For each configuration, 4 pumps were considered active; the 6 remaining pumps maintained shroud cooling but were otherwise inoperative.

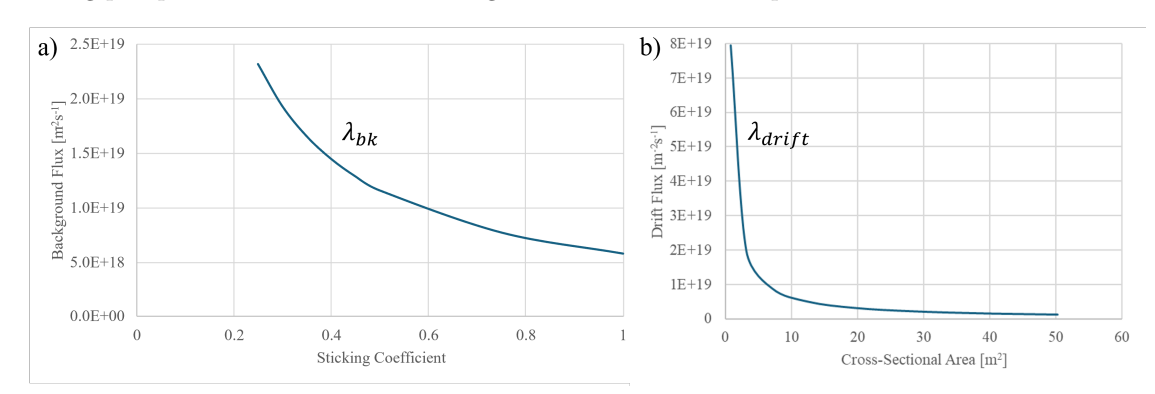


Figure 6: Neutral fluxes for a mass flow of 13.6 mg/s. (a) background flux λ_{bk} as a function of sticking coefficient for $10.8m^2$ pumping area; values are present in Table 1. (b) Drift flux λ_{dr} as a function of facility cross-sectional area.

For the initial simulations, we examined the impact of changing the sticking coefficient for the pumps while maintaining the mass flow and pump configuration for each of the three configurations. For a mass flow of 13.6mg/s and a total pumping area of $10.8m^2$, the total particle flux required for extraction is $5.78 \times 10^{18} s^{-1} m^{-2}$; the background flux at the tested sticking coefficients is shown in Figure 6(a).



Tables 2 and 3 show the resulting simulated fluxes to thruster and pump surfaces. As seen in Figure 7(a), all thruster surfaces experience approximately the same flux at any given sticking coefficient in the 4 Downstream configuration. All mass inflow and extraction happens at the downstream face of the thruster or further downstream within the facility; as such, there is no drift across the thruster and thus no difference in flux experienced on thruster surfaces. Further, the upstream pumps (7 to 10) experience the same flux as the thruster surfaces for the same reason (Table 3). Of the six downstream pumps, four are active and two are not. The four active pumps (1, 2, 5, 6) experience similar fluxes that average to approximately the background flux for each sticking coefficient. The remaining two inactive pumps (3, 4) experience slightly higher flux than the active pumps but lower flux than the upstream surfaces. The flux to thruster surfaces and nearby inactive pumps is significantly higher than the background flux: initial analysis indicates a general gradient in flux moving away from the active pump surfaces, but the exact mechanism of this gradient has yet to be determined.

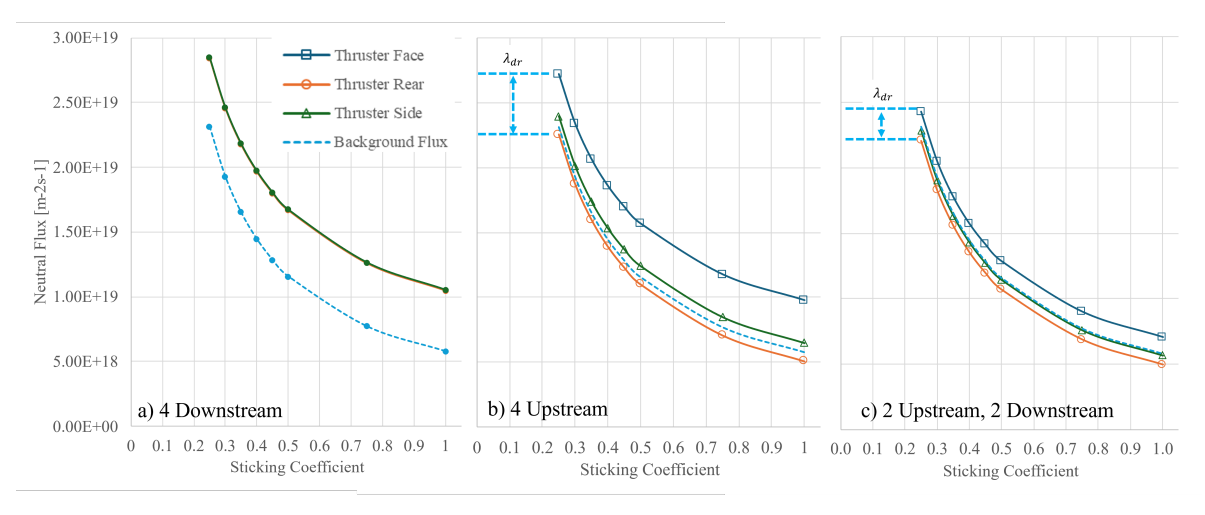


Figure 7: Comparison of neutral flux values to the front, rear, and right thruster surfaces and the background flux for the 4 Downstream (a), 4 Upstream (b), and 2 Up 2 Down (c) pump configurations. These results show that the presence of facility drift, λ_{dr} , is dependent on pumping and facility configuration but not directly dependent on a universal sticking coefficient.

For the 4 Up case, pumps 7, 8, 9, and 10 are active. Given that mass is released downstream of the thruster, we would therefore expect significant drift across the thruster face; this is observable by comparing the flux on thruster surface. For example, the right, left, top, and bottom surfaces experience approximate the same flux values, with a slight increase in flux to the bottom face due to the proximity of the thrust stand and floor (Figure 7(b),Table 4). However, the thruster face experiences significantly higher flux while the thruster rear experiences lower flux $(9.76 \times 10^{18} s^{-1} m^{-2} \text{ vs } 5.08 \times 10^{18} s^{-1} m^{-2} \text{ in the } \alpha_{sc} = 1.00 \text{ case})$. This difference between the thruster face and rear is $4.67 \times 10^{18} s^{-1} m^{-2}$ for all sticking coefficients. As the facility is approximately 2.36m in radius but contains a reduced cross-sectional area due to the floor and other structures, the expected drift across the chamber would be between $3.56 \times 10^{18} s^{-1} m^{-2}$ and $5.34 \times 10^{18} s^{-1} m^{-2}$; this places the flux differential between the face and rear of the thruster well within the expected drift range and implies the flux differential is due primarily or wholly to drift. The flux to the thruster side is slightly above the background flux; similarly to the 4 Downstream case, this may be due to a flux gradient that extends from the active pump surfaces to the far wall of the facility, though the exact dynamics of this gradient are still to be determined.

For pump surfaces, the active pumps are 7, 8, 9, and 10. The average flux to these active pumps is again approximately equal to the background flux for the experimental condition (Table 5). The downstream (inactive) pumps all experience significantly higher flux rates, ranging from an average of $7.7 \times 10^{18} s^{-1} m^{-2}$ above the upstream pumps for $\alpha_{sc} = 1.00$ to $8.1 \times 10^{18} s^{-1} m^{-2}$ above the upstream pumps for $\alpha_{sc} = 0.25$. The analytical relationship between these flux rates has yet to be determined. The flux to the thruster right side is approximately equal to the background flux and reflects the lack of a gradient in general background flux: in this configuration, mass is extracted almost equally at the front and rear of the facility, so the general background flux throughout the facility should be represented by the background flux.



For the third VTF-2 simulation, pumping was split between 2 upstream pumps (9 and 10) and 2 down-stream pumps (2 and 6); the resulting fluxes to thruster surfaces and pump surfaces are presented in Figure 7(c) and Tables 6 and 7 respectively. Again, there is a flux differential between the thruster front and rear; in this pumping configuration, the differential flux is $2.2 \times 10^{18} s^{-1} m^{-2}$, which is approximately half the differential from the 4 Upstream case and reflects that half the mass is extracted at the downstream location and therefore does not travel upstream. That the differential is slightly below $\frac{\lambda_{drift}}{2}$ can be partly correlated to the active upstream pumps experiencing average fluxes slightly lower than the active downstream pumps; the average overall flux to active pumps remains the same approximation of the background flux, but slightly more mass is extracted downstream than upstream. The inactive downstream pumps also show elevated fluxes in general compared to the active downstream pumps, but the exact cause of differences in flux to the pump surfaces has yet to be fully explored. It is likely that Pump 6 experiences higher flux than Pump 2 (both active) due to the open/exposed side pumping surface of Pump 6; this allows Pump 6 to experience more direct flux than Pump 2.

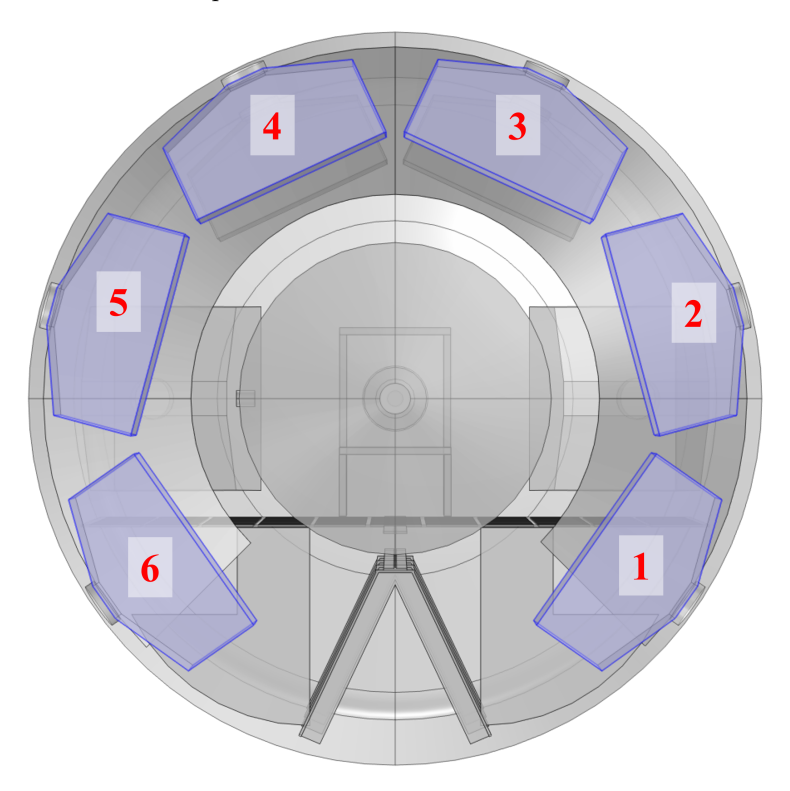


Figure 8: Cross-section of VTF-2, showing the 6 downstream pump positions.

The exchange of flux between pump surfaces likely also plays a role. As can be seen in Figure 8, Pump 4 is the only downstream pump that does not exchange particles directly with an active pump in this configuration; this may be the reason that Pump 4 experiences the highest flux of the downstream pumps. The remaining relationships have yet to be determined but are at least partly consequences of axial asymmetry of pump locations.

The inactive upstream Pumps 7 and 8 experience reduced flux relative to active Pumps 9 and 10. The difference is approximately the flux due to drift; as pumps 7 and 8 are oriented down towards the long axis of the chamber with their side surfaces oriented azimuthally, they will not directly experience drift traveling down the long axis and thus experience lower flux.

To summarize the effects of pumping conditions on the thruster, Figure 9 depicts the flux to the thruster face as a function of sticking coefficient for the three previously described pump configurations. An additional configuration in which the total number of pumps is doubled (thus doubling the pump surface area and reducing the background flux) was added. As can be seen in the graph, the flux to the thruster face for a sticking coefficient of 1.00 in the 2 Up 2 Down configuration is $7.07 \times 10^{18} s^{-1} m^{-2}$; doubling the pump area for the 4 Up 4 Down configuration reduces the flux to the thruster face to $4.37 \times 10^{18} s^{-1} m^{-2}$. Thus we can



see that the experience of the thruster is not necessarily linearly related to the pump surface area: doubling the area results in only a 43% decrease in flux to the thruster face. This nonlinearity is likely due to the drift through the facility which is not necessarily affected by total pump surface area, but further analysis is needed.

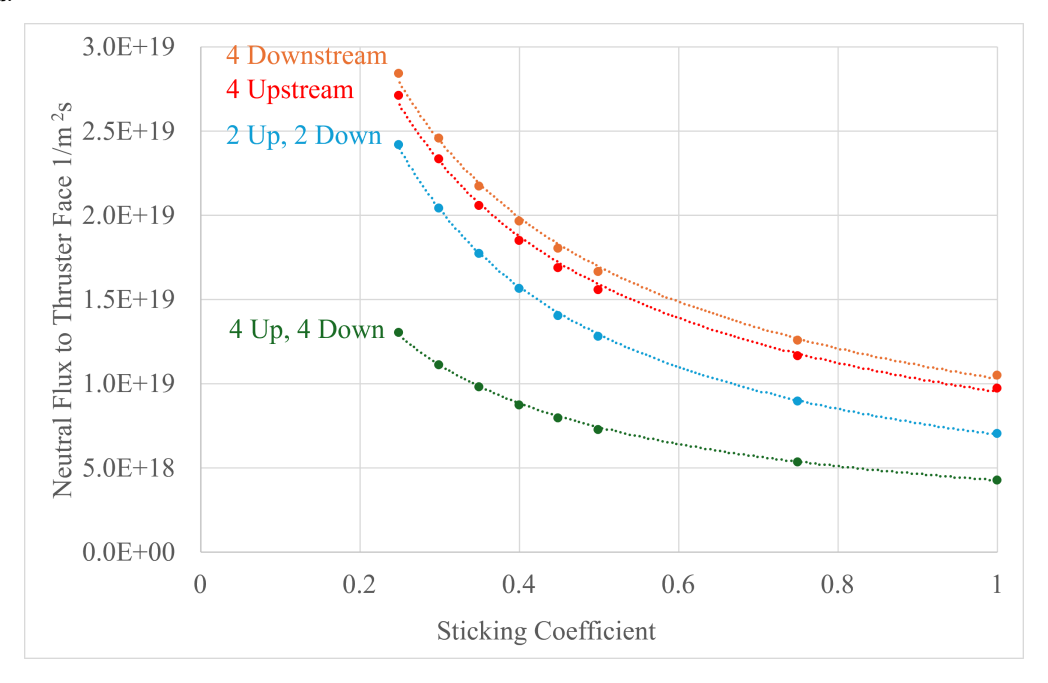


Figure 9: Comparison of neutral flux to the thruster face as a function of sticking coefficient for four different pumping schemes: 4 downstream pumps; 4 upstream pumps; 2 upstream and 2 downstream pumps; and 4 upstream and 4 downstream pumps.

B. VTF-2 vs LVTF

The presence of the converger in VTF-2 has the potential to impact neutral behavior within the facility. To study the impacts of facility geometry on overall neutral particle behavior, we simulated similar 4-pump configurations for VTF-2 and LVTF and compared the resulting fluxes. Because the pumps are identical between the facilities, maintaining the same number of pumps and similar relative positions should isolate any differences in thruster environments between the facilities to consequences of the facility geometry; the specific pump configurations were chosen to determine if such geometric consequences could be minimized.

Figure 10 and Table 8 show the flux measurements for representative surfaces in simulation for each pump configuration and sticking coefficient $\alpha_{sc}=0.25$. The flux to active pumps is constant in all cases and is approximately equal to the background flux from Table 1. In the 4 Downstream case, the thruster experiences slightly more variation in LVTF than in VTF-2, but the flux difference between the face, rear, and left varies by less than 2.5%. In the 4 Upstream case, the relative pattern of flux is maintained: the front experiences higher flux than the left, which in turn is higher than the rear. The flux differential in VTF-2 is again $4.67 \times 10^{18} s^{-1} m^{-2}$ as previously seen, while the differential in LVTF is $3.57 \times 10^{18} s^{-1} m^{-2}$; the difference is partially due to the difference in cross sections for the facilities, with LVTF having a larger radius in general.

The critical case is the 2 Upstream 2 Downstream case. Here we see that the fluxes to rear, left, and active pumps are approximately identical between VTF-2 and LVTF, while the flux to the thruster face in VTF-2 is only 1.4% higher than in LVTF. Again, this is partially due to an increase in the drift flux in VTF-2 due to its smaller cross-sectional area.



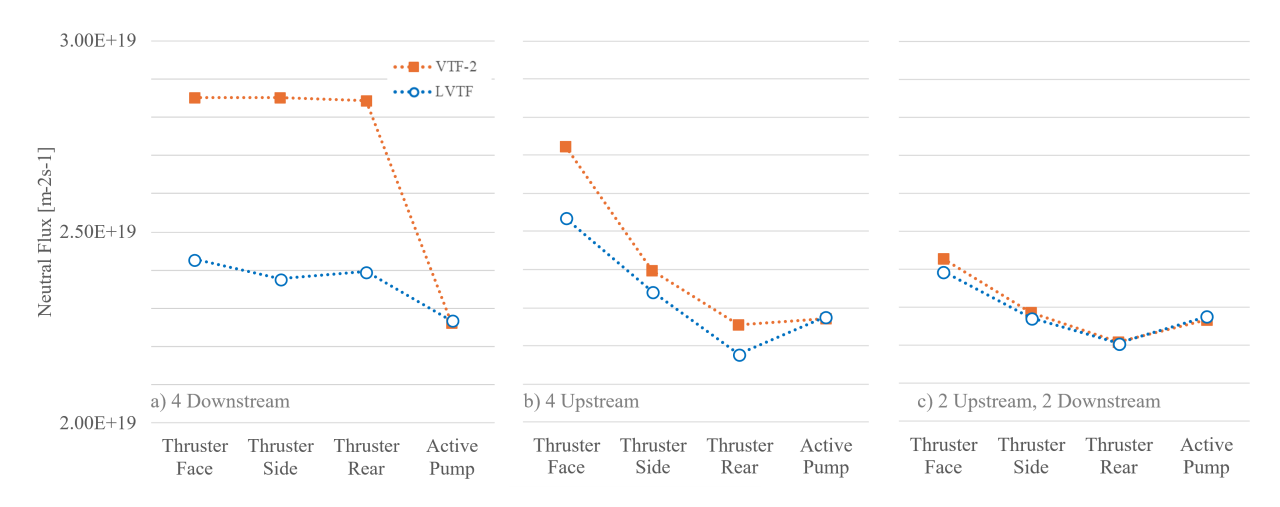


Figure 10: Comparison of neutral flux to thruster surfaces and active pump surfaces between VTF-2 and LVTF for the three pumping conditions shown in Fig 4: "4 Downstream" (a), "4 Upstream" (b), and "2 Up 2 Down" (c). These results show that the flux that would be measured by an ion gauge on the "Thruster Side" may give similar results, however, the flux to the "Thruster Face" can be considerably different, as shown in (a) and (c). Results in plot (c) show that appropriate selection of facility operation can result in matched neutral conditions across facilities. For reference, the active pump flux of $2.28E19m^{-2}s^{-1}$ would be measured by a vacuum gauge as approximately $16.5\mu Torr$.

V. Discussion

The 36 simulations conducted for this effort were executed with identical thruster operating conditions; only the facility characteristics were changed, through either pump sticking coefficients, active pump placement, the number of pumps active (in one case), or the facility geometry itself. Interaction between the thruster and the facility, including the fluxes described here, will lead to changes in thruster operation. However, the trends discussed herein are self-consistent: changes observed in the thruster's local environment are significant and predictable.

In the first finding, we note that the background flux varies with effective pumping capacity (sticking coefficient and total pump surface area) and mass flow only (see Eq. 2); changes to pump placement do not affect the background flux, only how that flux is applied within the facility. Related to the background flux is the drift flux at the thruster face, which drives the flux differential between thruster front and rear surfaces (see Eq. 4). While the exact relationships of these values to the thruster environment are still under investigation, quantifying and reporting these two values will help investigators translate results from one facility to another. Figure 11 presents a visual approximation of the relationships of neutral fluxes within a facility.

Secondly, as noted with Figure 9, the thruster environment does not appear to be linearly related to pumping capability. It is incorrect to assume that doubling the extraction rate within a facility will decrease the flux experienced by the thruster by one half. Drift flux is primarily a consequence of thruster mass flow, facility cross section, and the percent of mass extracted upstream of the thruster; contrary to what may be an intuitive expectation, increasing mass extraction upstream of the thruster may increase the flux experienced by the thruster through increased drift.

These analyses show that it may be possible to reach approximately the same near-thruster environments in two separate facilities through careful management of the pattern of mass extraction. Such management extends beyond simple matching of ion gauge measurements (usually reported as static pressure) near the thruster: while total flux for such a measurement may be similar, the proportions between background flux and drift flux may be different and lead to distinct impacts on different facility effects. For example, in Figure 10, the flux to the thruster face in the 2 Up 2 Down scenario for VTF-2 approximately matched the flux in the 4 Downstream scenario for LVTF; however, the fluxes to the side and rear of the thruster were different, suggesting that the ambient background density in the LVTF 4 Downstream case was higher than in the VTF-2 2 Up 2 Down case. This background density change could lead to differences in charge and



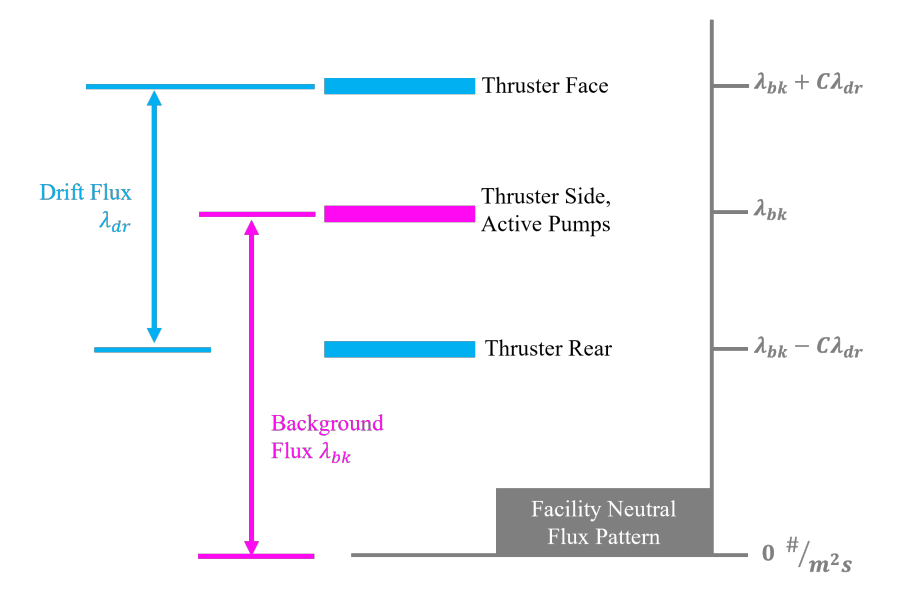


Figure 11: Summary of the initial analytical representation of neutral flux behavior within a facility. Active pumps and the thruster side will generally experience a flux approximately equal to the background flux. The thruster face and rear will experience a flux offset from the background flux by a portion of the drift flux (measured at the thruster) up or down respectively. Other effects on these fluxes due to chamber geometry and operational conditions are under investigation.

momentum exchange, beam divergence, electrical coupling, and other facility effects in spite of the similarity that a single flux measurement might indicate. ¹⁸

These results demonstrate a computational capability for facility design and optimization. Towards this goal, understanding the concepts of background flux and drift flux can help improve comparisons between facilities and efforts to translate facility operation to space conditions. These results support the common notion that increasing pumping capacity can improve facility performance, however, it is important to implement additional pumping in a way that effectively reduces unwanted facility effects such as flux to the thruster face and facility-borne neutral density in the plume.

VI. Conclusion

These results show the importance of considering vacuum facility flux behavior when comparing facility operation for EP devices. Neutral drift within the facility introduces a nonlinear response of flux to the thruster face when changing total pumping capacity and configuration. Using background flux and drift flux, we present the foundation for an analytical model for the neutral flux environment in the thruster region that can predict the flux to the thruster face and thus inform experimental and modeling efforts to quantify neutral-based facility effects. For future tests, it is strongly recommended that measured flux near the thruster must account for the facility drift flux to properly account for facility effects. Notably, our results show that the flux that would be measured by an ion gauge on the "Thruster Side" may give similar results, however, the flux to the "Thruster Face" can be considerably different. Through proper considerations, we show that the theory and modeling herein can be used to find facility operating conditions that can result in matched neutral conditions across facilities. The underlying analytical relationships can inform future facility design efforts to predict the impact of facility neutrals on thruster operation.

Future work will include further validation of these suggestions through experimentation and development of the full analytical model for approximating neutral flux conditions within a facility. These efforts will include improved experimental validation of the model and the observed trends. Further analytical studies will be undertaken to build analytical constructs for facility evaluation.



Appendix

Table 1: The background flux driven by $\dot{m}_{in}=13.6mg/s$ and $A_{pump}=10.8m^2$ for various sticking coefficients.

Sticking	background
Coefficient	flux
	$[s^{-1}m^2]$
0.25	23.1×10^{18}
0.30	19.3×10^{18}
0.35	16.5×10^{18}
0.40	14.5×10^{18}
0.45	12.8×10^{18}
0.50	11.6×10^{18}
0.75	7.71×10^{18}
1.00	5.78×10^{18}

Table 2: Neutral flux to thruster surfaces within VTF-2 while operating with only four downstream pumps active (4 Down condition). All flux values in $10^{18}s^{-1}m^{-2}$

Sticking		Thruster $[10^{18}s^{-1}m^{-2}]$									
Coefficient	Face	Rear	Right	Left	Top	Bottom					
0.25	28.5	28.4	28.5	28.5	28.5	28.6					
0.30	24.6	24.6	24.6	24.6	24.6	24.7					
0.35	21.8	21.8	21.8	21.8	21.8	21.9					
0.40	19.7	19.7	19.7	19.7	19.7	19.8					
0.45	18.1	18.0	18.1	18.1	18.0	18.1					
0.50	16.7	16.7	16.7	16.7	16.7	16.8					
0.75	12.6	12.6	12.6	12.6	12.6	12.7					
1.00	10.5	10.5	10.5	10.5	10.5	10.6					

Table 3: Neutral flux to pump surfaces within VTF-2 while operating with only four downstream pumps active (4 Down condition). All flux values in $10^{18}s^{-1}m^{-2}$

Sticking		Pumps $[10^{18}s^{-1}m^{-2}]$									
Coefficient	1	2	3	4	5	6	7	8	9	10	
0.25	23.0	22.3	23.6	23.6	22.3	23.0	28.4	28.4	28.4	28.4	
0.30	19.2	18.5	19.8	19.8	18.5	19.2	24.5	24.5	24.6	24.6	
0.35	16.5	15.8	17.0	17.0	15.8	16.5	21.7	21.7	21.8	21.8	
0.40	14.5	13.8	15.0	15.0	13.8	14.5	19.6	19.6	19.6	19.6	
0.45	12.9	12.3	13.3	13.3	12.3	12.9	18.0	18.0	18.0	18.0	
0.50	11.6	11.0	12.0	12.0	11.0	11.6	16.6	16.6	16.7	16.7	
0.75	7.79	7.31	8.12	8.12	7.31	7.79	12.6	12.6	12.6	12.6	
1.00	5.87	5.46	6.13	6.13	5.46	5.86	10.4	10.4	10.5	10.5	

Table 4: Neutral flux to thruster surfaces within VTF-2 while operating with only four upstream pumps active (4 Up condition). All flux values in $10^{18}s^{-1}m^{-2}$

Sticking		Thruster $[10^{18}s^{-1}m^{-2}]$									
Coefficient	Face	Rear	Right	Left	Top	Bottom					
0.25	27.2	22.5	24.0	24.0	23.7	24.3					
0.30	23.4	18.7	20.1	20.1	19.9	20.4					
0.35	20.6	16.0	17.4	17.4	17.1	17.7					
0.40	18.6	13.9	15.3	15.3	15.0	15.6					
0.45	17.0	12.3	13.7	13.7	13.4	14.0					
0.50	15.7	11.0	12.4	12.4	12.1	12.7					
0.75	11.8	7.08	8.50	8.50	8.22	8.77					
1.00	9.76	5.08	6.49	6.50	6.23	6.77					

Table 5: Neutral flux to pump surfaces within VTF-2 while operating with only four upstream pumps active (4 Up condition). All flux values in $10^{18}s^{-1}m^{-2}$

Sticking		Pumps $[10^{18}s^{-1}m^{-2}]$									
Coefficient	1	2	3	4	5	6	7	8	9	10	
0.25	30.6	30.9	31.0	31.0	30.9	30.6	21.8	21.8	23.6	23.6	
0.30	26.7	27.1	27.2	27.2	27.1	26.7	18.0	18.0	19.8	19.8	
0.35	24.0	24.3	24.4	24.4	24.3	24.0	15.4	15.4	17.1	17.1	
0.40	21.9	22.3	22.4	22.4	22.3	21.9	13.4	13.4	15.0	15.0	
0.45	20.3	20.7	20.8	20.8	20.7	20.3	11.8	11.8	13.4	13.4	
0.50	19.0	19.4	19.5	19.5	19.4	19.0	10.6	10.6	12.1	12.1	
0.75	15.1	15.4	15.5	15.6	15.4	15.1	6.89	6.88	8.26	8.26	
1.00	13.1	13.4	13.6	13.6	13.4	13.1	5.06	5.06	6.31	6.30	

Table 6: Neutral flux to thruster surfaces within VTF-2 while operating with two upstream and two down-stream pumps active (2 Up, 2 Down condition). All flux values in $10^{18}s^{-1}m^{-2}$

Sticking		Thruster $[10^{18}s^{-1}m^{-2}]$										
Coefficient	Face	Rear	Right	Left	Top	Bottom						
0.25	24.3	22.1	22.9	22.9	22.9	22.9						
0.30	20.5	18.3	19.1	19.1	19.1	19.1						
0.35	17.8	15.6	16.3	16.3	16.3	16.3						
0.40	15.7	13.5	14.3	14.3	14.3	14.3						
0.45	14.1	12.0	12.7	12.7	12.7	12.7						
0.50	12.9	10.7	11.4	11.4	11.4	11.4						
0.75	9.01	6.86	7.61	7.61	7.61	7.61						
1.00	7.07	4.94	5.68	5.68	5.68	5.68						



Table 7: Neutral flux to pump surfaces within VTF-2 while operating with two upstream and two downstream pumps active (2 Up, 2 Down condition). All flux values in $10^{18}s^{-1}m^{-2}$

Sticking		Pumps $[10^{18}s^{-1}m^{-2}]$									
Coefficient	1	2	3	4	5	6	7	8	9	10	
0.25	22.7	22.4	23.0	24.3	23.1	23.2	22.3	22.3	22.6	22.6	
0.30	19.0	18.6	19.3	20.5	19.3	19.4	18.5	18.5	18.8	18.8	
0.35	16.3	16.0	16.6	17.8	16.6	16.7	15.8	15.8	16.1	16.1	
0.40	14.3	14.0	14.5	15.8	14.6	14.7	13.8	13.8	14.0	14.0	
0.45	12.7	12.4	13.0	14.2	13.0	13.1	12.2	12.2	12.5	12.5	
0.50	11.4	11.2	11.7	12.9	11.8	11.8	10.9	10.9	11.2	11.2	
0.75	7.67	7.46	7.96	9.03	8.00	8.01	7.10	7.11	7.39	7.38	
1.00	5.78	5.62	6.07	7.06	6.11	6.10	5.20	5.20	5.49	5.48	

Table 8: Comparison of neutral fluxes to representative surfaces within VTF-2 and LVTF for $\alpha_{sc}=0.25$. All values in $10^{19}s^{-1}m^{-2}$

	4 Down	stream	4 Ups	tream	2 Up 2 Down		
	VTF-2 LVTF		VTF-2	LVTF	VTF-2	LVTF	
Thruster Face	2.85	2.43	2.72	2.53	2.43	2.39	
Thruster Rear	2.84	2.40	2.25	2.18	2.21	2.21	
Thruster Left	2.85	2.38	2.40	2.34	2.29	2.27	
Active Pump	2.26	2.27	2.27	2.28	2.27	2.28	



Acknowledgments

The authors acknowledge support from the Joint Advanced Propulsion NASA Space Technology Research Institute. This work was funded by Joint Advanced Propulsion Institute 20-STRI-FULL-0004, NASA Grant Number 80NSSC21K1118.

References

¹T Randolph, V Kim, H Kaufman, K Kozubsky, V Zhurin, and M Day. Facility effects on stationary plasma thruster testing. In 23rd International Electric Propulsion Conference, number 844, pages 13–16. The Electric Rocket Propulsion Society Worthington, OH, 1993.

²John W Dankanich, Mitchell Walker, Michael W Swiatek, and John T Yim. Recommended practice for pressure measurement and calculation of effective pumping speed in electric propulsion testing. *Journal of Propulsion and Power*, 33(3):668–680, 2017.

³RD Hazeltine. Transport theory in the collisionless limit. *Physics of Plasmas*, 5(9):3282–3286, 1998.

⁴GL Saksaganskii. Molecular flow in complex vacuum systems. (No Title), 1988.

⁵P Ossipov. The angular coefficient method for calculating the stationary molecular gas flow for arbitrary reflection law. *Vacuum*, 48(5):409–412, 1997.

⁶Richard Wirz and Ira Katz. A preliminary 2-d computational model of an ion thruster discharge chamber. In 39th AIAA/ASME/SAE/ASEE Joint Propulsion Conference and Exhibit, page 5163, 2003.

⁷JM Labello, HS Lowry, LM Smith, TM Moeller, and CG Parigger. Modeling of molecular flux in a space simulation chamber. *Int Rev Atom Mol Phys*, 2(2):85–91, 2011.

⁸Matteo Calafà. Characterization of the angular coefficient method on 2d and 3d piecewise smooth boundaries. *Computational and Applied Mathematics*, 43(8):450, 2024.

⁹Pietro Parodi, Zuheyr Alsalihi, and Thierry Magin. Smarta: A code based on the view-factor method for collisionless flows. In *AIP conference proceedings*, volume 2996, page 060007. AIP Publishing LLC, 2024.

¹⁰Roddam Narasimha. Collisionless expansion of gases into vacuum. Journal of Fluid Mechanics, 12(2):294–308, 1962.

¹¹Chunpei Cai, Iain D Boyd, and Quanhua Sun. Rarefied background flow in a vacuum chamber equipped with one-sided pumps. *Journal of thermophysics and heat transfer*, 20(3):524–535, 2006.

¹²Jason D Frieman, Thomas M Liu, and Mitchell LR Walker. Background flow model validation with a six-kilowatt hall effect thruster. *Journal of Propulsion and Power*, 36(2):308–311, 2020.

¹³Ehsan E. Taghizadeh, Richard A. Obenchain, Luke K. Franz, and Richard E. Wirz. Electric propulsion facility optimization via reduced order modeling. In 38th International Electric Propulsion Conference, pages IEPC-2024-588, 2024.

¹⁴Samuel J Araki. Radiosity view factor model for sources with general distribution. *Journal of Computational Physics*, 406:109146, 2020.

¹⁵Austen Thomas, Kristina Lemmer, Janice Cabrera, Mitchell LR Walker, Tyler Topham, and John Foster. High-speed far-field energy measurements in a 9-kw hall effect thruster for model inference and calibration. In 38th International Electric Propulsion Conference, 2024.

¹⁶Eric A Viges, Benjamin A Jorns, Alec D Gallimore, and JP Sheehan. University of michigan's upgraded large vacuum test facility. In 36th International Electric Propulsion Conference, pages 1–18, 2019.

¹⁷Charles Lipscomb, Iain D Boyd, Kaelan B Hansson, Joshua Eckels, and Alex Gorodetsky. Simulation of vacuum chamber pressure distribution with surrogate modeling and uncertainty quantification. In AIAA SCITECH 2024 Forum, page 2369, 2024.

¹⁸Richard A. Obenchain, Tyler Topham, Sophia Bergmann, John Foster, and Richard E. Wirz. Charge exchange (cex) corrections for electric propulsion facilities. In 39th International Electric Propulsion Conference, pages IEPC–2025–609, 2025.

